^{1}H and ^{15}N Dynamic Nuclear Polarization Studies of Carbazole

Jian Z. Hu,[†] Mark S. Solum,[‡] Robert A. Wind,[§] Brad L. Nilsson,[||] Matt A. Peterson,[||] Ronald J. Pugmire,*[,||] and David M. Grant[†]

Departments of Chemistry and Chemical and Fuels Engineering, University of Utah, Salt Lake City, Utah 84112, Environmental and Molecular Sciences Laboratory, Battelle Pacific Northwest National Laboratory, P.O. Box 999, MS K8-98, Richland, Washington 99352, Department of Chemistry, Brigham Young University, Provo, Utah 84602

Received: October 26, 1999

^{15}N NMR experiments, combined with dynamic nuclear polarization (DNP), are reported on carbazole doped with the stable free radical 1,3 bisdiphenylene-2-phenylallyl (BDPA). Doping shortens the nuclear relaxation times and provides paramagnetic centers that can be used to enhance the nuclear signal by means of DNP so that ^{15}N NMR experiments can be done in minutes. The factors were measured in a 1.4 T external field, using both unlabeled and 98% ^{15}N labeled carbazole with doping levels varying between 0.65 and 5.0 wt % BDPA. A doping level of approximately 1 wt % produced optimal results. DNP enhancement factors of 35 and 930 were obtained for ^{1}H and ^{15}N, respectively making it possible to perform ^{15}N DNP NMR experiments at the natural abundance level.

Introduction

The ^{15}N isotope has a spin 1/2 and, like ^{13}C, the chemical shift and chemical shift tensor principal values can be related to molecular structure. The large chemical shift range of the ^{15}N isotope (∼1100 ppm) provides an enhanced sensitivity to molecular structure variations and intermolecular interactions that exceeds other first row elements. However, the detection of a ^{15}N NMR signal in the solid state is very difficult due to a combination of low natural abundance, low gyromagnetic ratio, and the long spin−lattice relaxation time of this isotope. Hence, only limited amounts of data have been acquired in the solid state on the nitrogen shift and their principal shift values in nitrogen heterocycles.[1−6]

Increased sensitivity results from isotopic labeling and sample doping with a relaxation agent to reduce the recycle delay time. Further, a third signal enhancement alternative, dynamic nuclear polarization (DNP), has been known[7−11] for a number of years. This technique can be applied in solids containing both magnetic nuclei and unpaired electrons (present either by nature or by doping the solid with a suitable stable free radical). Polarization transfer can be induced between the electron and nuclear spin systems by irradiating at or near the electron Larmor frequency resulting in an enhanced nuclear polarization and, hence, a greater NMR signal. In principle, larger NMR signal enhancements may be obtained via DNP where the theoretical maximum enhancement is the ratio of the gyromagnetic ratios of the electrons and the nuclei. For example, for ^{1}H, ^{13}C, and ^{15}N nuclei the maximum enhancement factors are 660, 2600, and 6500, respectively. In practice these large theoretical enhancements are unrealized for a variety of reasons but enhancements of 1−3 orders of magnitude have been observed. Thus, the measurement time of an experiment can be significantly reduced.[10−25] Moreover, if the DNP condition can be achieved by appropriately doping the solid with paramagnetic centers, the nuclear relaxation time is generally reduced and an additional reduction of the experimental measuring time is achieved.

DNP NMR spectroscopy in solids has focused mainly on protons and ^{13}C nuclei. Recently, preliminary ^{15}N DNP experiments were reported in doped benzamide,[26] but the ^{15}N DNP enhancement could only be estimated (ca. 260) as the signal in the absence of the DNP condition could only be approximated with the instrumentation available at that time. Griffin and coworkers have reported a ^{15}N DNP enhancement of 50 at 40 K in a glycerol solution of ^{15}N Ala-labeled T4 lysozyme doped with 4-amino-TEMPO.[23]

In this paper a systematic DNP/NMR study is reported of the ^{1}H and ^{15}N nuclei in ^{15}N labeled carbazole, a model compound representing one of the common nitrogen heterocycles found in fossil fuels. This investigation includes measuring: (1) the changes in the ^{1}H spin−lattice relaxation times in the laboratory and rotating frames for carbazole after doping the sample with various amounts of the free radical; (2) the ^{1}H and ^{15}N DNP enhancement factors; (3) the effects of the doping upon the ^{1}H and ^{15}N DNP polarization curves; and (4) comparison of the ^{15}N shift tensor principal values at 1.4 T under conditions of DNP-CP, DNP-SP as well as CP at 4.7 T. The spin-labeled material ensures that accurate values for the unenhanced ^{15}N signal can be measured. These experiments demonstrate that large signal enhancements can be observed in this case and that one can obtain useful powder patterns under DNP experimental conditions that duplicate those obtained under standard NMR conditions.

Experimental Section

1. Sample Doping. The ^{15}N labeled carbazole was doped with the stable radical 1,3-bisdiphenylene-2 phenylallyl (BDPA) using the solvent-evaporation method,[27] i.e., both the carbazole and BDPA were dissolved in acetone, after which the acetone was allowed to evaporate slowly. This method of sample doping

* Author to whom correspondence should be sent.
[†] Department of Chemistry, University of Utah.
[‡] Department of Chemical and Fuels Engineering, University of Utah.
[§] Battelle Pacific Northwest National Laboratory.
[||] Brigham Young University.

10.1021/jp9938011 CCC: $19.00
Published on Web 04/19/2000

SCHEME 1[a]

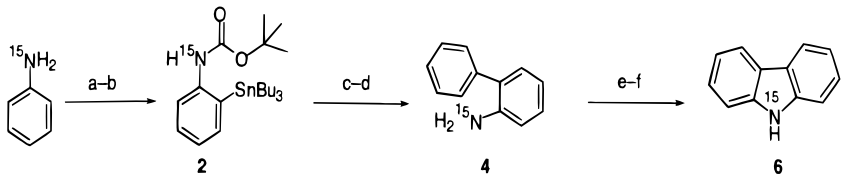

[a] Reagents: (a) $(BOC)_2O$, K_2CO_3, THF-H_2O (1:1); (b) i. tBuLi, THF, −78 °C to −20 °C, ii. Bu_3SnCl, −78 °C to 25 °C; (c) bromobenzene, $Pd(Ph_3)_2Cl_2$; (d) 4 M HCl; (e) i. $NaNO_2$ (aq), AcOH; ii. NaN_3; (f) 180 °C.

has proven to be a very useful way to dope crystalline materials. Four samples were prepared with doping levels of 0.65, 1.1, 2.5, and 5.0 wt % BDPA.

2. DNP Spectrometer. The DNP NMR spectrometer operates at a field of 1.4 T, corresponding to electron, ^{1}H, and ^{15}N Larmor frequencies of 40 GHz, 60 MHz, and 6 MHz, respectively. The NMR components of the spectrometer consist of a Chemagnetics CMX-100 dual channel console. The magnet is a small-animal horizontal imaging 2.3 T superconducting magnet from Magnex, in which the field was reduced to 1.4 T. This magnet has a clear bore diameter of 22 cm, which readily accommodates the construction of the DNP NMR probes.[28] Microwave irradiation is achieved with a Wiltron microwave frequency generator, model 68263B, capable of producing an output of 6 dBm in the frequency range 20−40 GHz. The output traveling wave tube amplifier (Logimetrics model A400/KA) amplifies the microwave power to 10 W c.w. in the frequency range 26−40 GHz. Compared with fixed-frequency sources such as klystrons, this setup has an important advantage. Both the EPR spectrum and the DNP enhancement curve can be determined and optimized by sweeping the microwave frequency rather than the field, thereby avoiding the construction and calibration of special field-sweep coils in the magnet. It also avoids the necessity of continual adjustment of the probe tuning at the different field strengths since the NMR resonance frequencies remain unaffected by sweeping the microwave field. A further advantage is that the microwave frequency and microwave pulses are under computer control through a GPIB interface board and are synchronized with the NMR pulse sequence. This arrangement fully automates the measurement of the DNP enhancement curve (i.e., the DNP enhancement factor as a function of microwave frequency). Furthermore, the capability of generating a pulsed microwave field allows lossy samples to be investigated.

The DNP probe is home-built, and is capable of performing DNP NMR on static samples in the temperature range of 110−350 K. The NMR coil is a 5-turn solenoid coil with an inner diameter of 10.5 mm and length of 11 mm made of 1 mm copper wire. The setup can be double tuned to ^{1}H and a second nucleus of interest (^{15}N in this case). This setup is a variant of previous designs.[10,16,29,30] The microwave irradiation is introduced into the sample using a combination of a cylindrical horn antenna and a movable reflector. The NMR coil axis is coincident with that of the horn antenna. The copper reflector is placed approximately half a wavelength (about 3.5 mm) away from the other end of the NMR coil so that the decrease in the quality factor of the NMR coil is minimized. In this way both the microwave and the NMR efficiency can be optimized. It is estimated that with this design the 10 W incident microwave power corresponds to an average amplitude of the microwave field in the sample of about 0.04 T (rotating component). In nonlossy samples, such as doped polystyrene, DNP enhancements were obtained comparable to those previously reported on considerably smaller samples.[10,31] The DNP probe is equipped with two modulation coils (a SR850 DSP lock-in amplifier from Stanford Research Systems operating at a modulation frequency of 100 kHz) which, in combination with the microwave frequency sweep, makes it also possible to obtain c.w. first-derivative 40 GHz EPR spectra.

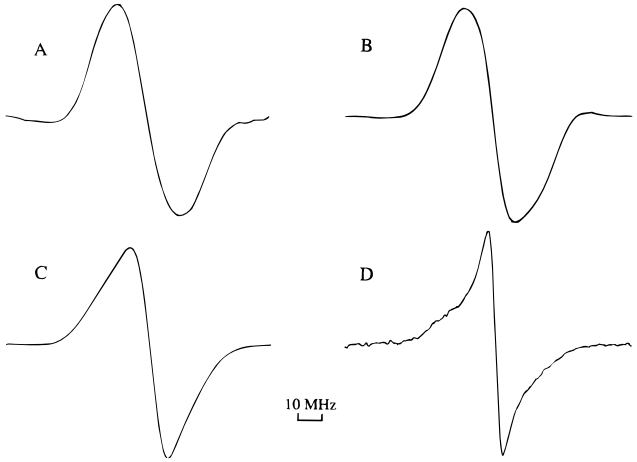

Figure 1. The 40 GHz EPR spectra for carbazole samples doped with BDPA. The doping levels are A: 0.65; B: 1.1; C: 2.5; and D: 5.0% (w/w).

3. NMR and DNP NMR Experiments. Unless stated otherwise, the experiments were performed at room temperature. The ^{1}H DNP enhancement factors and the relaxation times in the laboratory and rotating frames were measured with standard single pulse wide-line NMR techniques using RF fields of 64 kHz. This field was also used for decoupling. ^{15}N single (90°) pulse and ^{1}H-^{15}N cross-polarization (CP) experiments, with and without microwave irradiation, were performed using ^{15}N and ^{1}H RF fields of 48 kHz during CP, and a ^{1}H field of 64 kHz during decoupling. To eliminate distortions resulting from acoustic ring-down after the ^{15}N RF irradiation, a τ-180-τ echo sequence was employed, with a delay time τ of 150 μs.

Finally the effects of radical doping on isotropic and anisotropic chemical shifts and/or its spectral resolution has been investigated. This is done by performing standard ^{13}C and ^{15}N CP experiments, with and without MAS, on the doped and undoped ^{15}N labeled carbazole samples. A Chemagnetics CMX-200 spectrometer was used for these measurements.

4. Synthesis of ^{15}N Labeled Carbazole. ^{15}N labeled carbazole was synthesized according to Scheme 1.[32]

Results and Discussion

1. EPR and ^{1}H DNP NMR. The first derivative EPR spectra for the four doped carbazole samples are given in Figure 1. At the two lowest doping levels (Figure 1A and 1B) a single ESR line is observed with a near Gaussian line shape and a width of approximately 26 MHz (full width at half-maximum), typical results for diluted radicals in solids.[31] At the 2.5% doping level (Figure 1C), the EPR spectrum consists of two overlapping lines,

TABLE 1: EPR and ^{1}H-NMR Parameters of the Carbazole Samples Studied[a]

wt %	$N_e \times {}_{10}{}^{-19}$ (g^{-1})	$N_{e'} \times {}_{10}{}^{-19}$ (g^{-1})	$T_{1\rho}$ (ms)	T_{1S} (s)	M_{0S} (%)	T_{1L} (s)	M_{0L} (%)	$N_e \times T_{1S}$	$N_e \times T_{1L}$	E-1
0 (undoped)	0	0	>500	137	18	1074	82	0	0	0
0.65	0.41	0.94	12.0	1.6	34	17.5	66	0.66	7.18	32
1.1	0.8	1.6	3.4	1.0	55	12.0	45	0.80	9.60	35
2.5	1.9	3.6	1.9	0.33	58	3.1	42	0.63	5.89	23
5.0	4.3	7.2	0.8	0.12	65	1.38	35	0.52	5.93	15

[a] N_e = measured concentration of unpaired electrons; $N_{e'}$ = the calculated unpaired electron concentration based on the amount of BDPA used to dope the samples; T_{1S}, T_{1L} = the proton spin−lattice relaxation time, measured at an external field of 1.4 T and without the presence of microwave irradiation; $T_{1\rho}$ = the average proton rotating frame relaxation time, measured in a lock field of 64 KHz and an external field of 1.4 T under the DNP condition; E-1 = the proton DNP enhancement factor at the frequencies of the solid state effect, observed when irradiating with a microwave frequency equal to the difference between the electron and ^{1}H Larmor frequencies.

one with a width similar to that observed at the lower doping levels, and one with a width of about 14 MHz. This is probably an indication that the radicals are not homogeneously distributed throughout the sample, and that a portion of the free radicals are present in agglomerates where the electrons are so close to each other that spin-exchange narrowing occurs.[7] At the 5% doping level the percentage of the component with broad line width (~26 MHz) decreases, and the line width of the narrow component is reduced to about 6 MHz (Figure 1D). An EPR line width of about 5 MHz for pure BDPA was obtained under the same experimental conditions (the same EPR power and modulation power). This result indicates that a substantial portion of the radicals are clustered together at 5% doping levels. The unpaired electron concentration, N_e, was measured on the 40 GHz DNP/ESR spectrometer using polystyrene doped with BDPA with a known free radical concentration of 1.6×10^{19} g^{-1} as a calibration standard. The measured N_e is about half of the calculated free radical concentration based on the amount of BDPA added by the doping procedure.

Table 1 contains the ^{1}H spin−lattice relaxation times in the laboratory and rotating frame, T_1 and $T_{1\rho}$, respectively, of the undoped and doped samples. The T_1 measurements were made with and without DNP enhancement while only the T_1 values obtained without DNP are reported in Table 1. It was found that the ^{1}H T_1 values obtained with and without DNP enhancement agree with each other within the experimental error. However, the relative contributions from the multiple relaxation components contributing to the magnetization may change because the DNP enhancement factor is different for different components. Conversely, the $T_{1\rho}$ measurements were made on the DNP-enhanced signals in order to take advantage of the increased sensitivity available.

In the T_1 measurements the ^{1}H magnetization as a function of the recovery time is multiexponential but can be expressed with a high degree of confidence by the following equation consisting of two exponential components,

$$M(t) = M_{0S}(1 - \exp(-(t/T_{1S}))) + M_{0L}(1 - \exp(-(t/T_{1L}))) \quad (1)$$

where T_{1S} and T_{1L} denote the components with short and long T_1 relaxation times, respectively, and $M_{0S} + M_{0L} = 1$. The two relaxation rates differ by an order of magnitude. In a related study on dibenzofuran (DBF)[27b,33] it was noted that the ^{1}H T_1 in DBF also displays multiexponential behavior in which the value of the short T_1 component is an order of magnitude smaller than that of the longer T_1 component. The relaxation mechanism for the longer component arises from dipolar interactions among the protons. A rigid lattice environment, i.e., $\omega_H\tau_c \gg 1$, commonly gives rise to a rather long ^{1}H T_1 value. However, a short ^{1}H T_1 component is usually also noted in crystalline solids and is thought to be due to mobilized species in the lattice arising from lattice defects. These so-called mobilized species, on the order of 1% or less, can be directly observed by delayed acquisition MAS experiments.[34] These mobilized species act as relaxation sinks which relax proximate protons by a spin-diffusion process. Consequently, a shorter ^{1}H T_1 value is observed in these nuclei.

TABLE 2: Parameters Relevant to Define the Diffusion Limits

wt %	$N_e \times 10^{-19}$ (g^{-1})	$N_e \times 10^{-19}$ (cm^{-3})	R (Å)	b (Å)	β (Å)
0.65	0.41	0.526	35.7	7	7.33
1.1	0.8	1.028	28.5	7	7.33
2.5	1.9	2.442	21.4	7	7.33
5.0	4.3	5.526	16.3	7	7.33

The spin−lattice relaxation data are complicated by the presence of free radicals in the doped samples. A useful model for describing this behavior consists of a diffusion limit defined by the diffusion barrier, b, the scattering radius, β, and a radius, R, that may be related to the average distance between electrons when the relationship $(4/3)\pi R^3 N^e = 1$ holds.[35−38] Within the distance, b, between a nucleus and the unpaired electron, (i.e., $r < b$) the electron−nuclear dipolar interaction is sufficiently large that spin diffusion among the nuclei is quenched, and the protons are unobservable. Within the scattering radius, i.e., $r < \beta$, proton relaxation is governed primarily by direct electron−proton interactions, whereas for $r > \beta$ proton relaxation is governed by proton−proton spin diffusion until a proton closer to the free electron is encountered. Wind et al.[38] have provided a detailed analysis of this model. Complete spin diffusion holds if $b \leq \beta$ and all observable protons relax exponentially with a uniform average relaxation rate. Limited spin diffusion (LSD) holds if $b < \beta < R$ and within this limit, for protons at a distance $b < r < \beta$, a distribution of relaxation rates is obtained. The long-term relaxation exhibits exponential behavior and is governed by the protons at a distance $\beta < r < R$.

Duijvestijn et al.[31] have determined that b is equal to 7 Å in polystyrene doped with BDPA. It is reasonable to assume the same b value in the case of carbazole doped with BDPA. The carbozole unit cell contains 4 molecules,[39] with cell volume of 825.3 cubic Å and density of 1.285 g/cm^3. The average volume for one proton is thus 22.9 Å^3. The diameter of the sphere for each proton is 3.53 Å which is the average distance (lattice constant) between the protons in carbazole. Given the Larmor frequency (60 MHz) for protons, β is found to be 7.33 Å by following the calculation given by Wind et al.[38] Using the experimentally determined radical concentration and assuming a homogeneous distribution of radicals, the R-values for the four doped samples are easily calculated and the results are given in Table 2.

It is known from Table 2 that the condition $R \gg \beta \approx b$ is satisfied for the four doped samples. Consequently, the argument for complete spin-diffusion[35−38] is valid in the doped carbazole

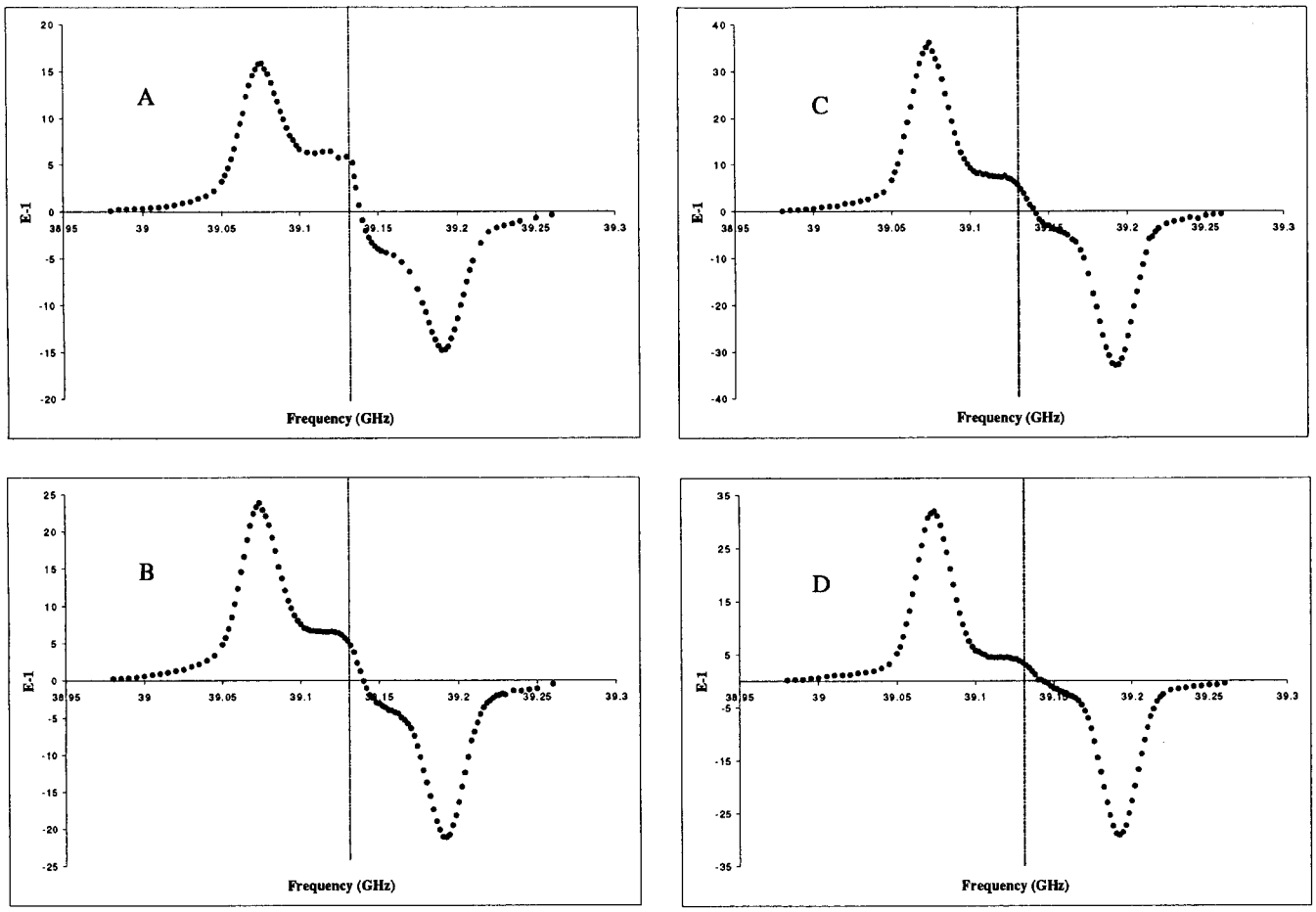

Figure 2. The proton DNP enhancement factor (E-1) as a function of microwave irradiation frequency $\omega - \omega_e$ for carbazole doped with BDPA at A: 5 wt %; B: 2.5 wt %; C: 1.1 wt %; D: 0.65 wt %.

samples. To explain the biexponential spin−lattice relaxation behavior, one must assume an inhomogeneous distribution of the BDPA radicals in the sample. The doped samples can be approximated by two or more types of domains, where one domain is enriched in BDPA compared to other domains. Visual inspection supports this postulate as one can clearly see a heterogeneous distribution of BDPA in the most highly doped sample. Whenever complete spin-diffusion is valid, a single-exponential relaxation time is obtained for protons located inside the same domain. This relaxation in the enriched domain is faster because the proton T_1 is inversely proportional to the radical concentration. For doping levels less than 2.5%, both T_{1S} and T_{1L} are inversely proportion to the radical concentration (see Table 1). Significant deviations are found at the 5% doping level as a consequence of radical clustering. These deviations are consistent with EPR distortions noted in Figure 1d.

In the doped samples, $T_{1\rho}$ was also found to be nonexponential (in the undoped sample the rotating frame relaxation time is so long that only a lower limit could be determined). Two to three exponential components are required to fit the rotating-frame relaxation data. This nonexponential behavior may also be attributed to heterogeneous domains with different radical concentrations. This heterogeneity precludes a detailed discussion of the data due to variability in the DNP enhancement factors. Only the average values of $T_{1\rho}$ are given in Table 1. These $T_{1\rho}$ values are approximated from a first-order decay law from the time required for signal decay to its half-maximum intensity and then divided by ln2.

Doping carbazole with BDPA reduces both the proton T_1 and $T_{1\rho}$ values by 2−3 orders of magnitude. The T_1 reduction is very advantageous as it reduces the pulse recycle time. However, the reduction in $T_{1\rho}$ is less desirable, as it limits the contact time that can be used in a CP experiment, which typically should be of the order of 1−5 ms in ^{1}H-^{15}N CP experiments. Hence, it may be concluded that the doping levels should not exceed approximately 1 wt % in order to minimize serious signal losses in the CP experiment.

TABLE 3: Parameters Obtained on Carbazole Samples Doped with Different Concentrations of BDPA[a]

sample	solid state			thermal mixing	Overhauser	
wt% BDPA (g^{-1})	ω_s	$\Delta_{1/2}$	E-1	E-1	ω_e	E-1
0.65	59.3	28	32	3	39.133	4
1.1	59.3	29	35	6	39.133	5
2.5	58.8	31	23	5	39.133	4
5.0	57.9	33	15	7	39.133	4

[a] ω_s and $\Delta_{1/2}$ are in units of MHz. The unit ω_e is in GHz. E-1 denotes the absolute enhancement for each type of DNP mechanism. The value of ω_o was visually approximated at 20 MHz.

Figure 2 exhibits the ^{1}H DNP enhancement curves of the four doped samples. The enhancement curve presents the DNP enhancement factor, E-1 (the DNP-enhanced signal minus the thermal equilibrium signal)/ (the thermal equilibrium signal) as a function of the applied microwave frequency. Extensive reviews of the DNP mechanisms and the resulting enhancement curves have been published elsewhere[7−11,31] and the functional forms of the enhancement mechanisms will not be repeated. However, a brief summary of the main results on carbazole provides valuable information on the factors contributing to the enhanced signals.

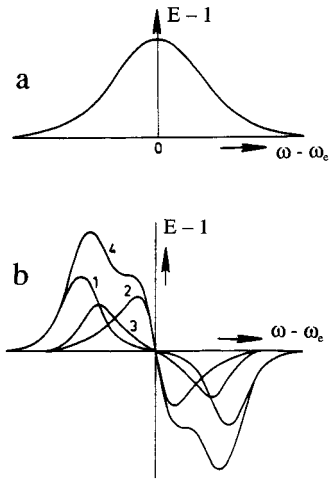

Figure 3. Example of E-1 as a function of $\omega - \omega_e$ for (a) the Overhauser effect where DNP is due to time dependent nuclear electron interactions and (b), other interactions where DNP is due to fixed paramagnetic centers; 1: solid-state effect; 2: direct thermal mixing effect; 3: indirect thermal mixing effect; 4: overall enhancement. The data for this figure were taken from the work of Wind et al.[10]

It is clear that the enhancement curves are essentially antisymmetrical around the electron Larmor frequency and become maximal when the microwave frequency equals the sum or the difference of the electron and the proton Larmor frequencies, $\omega = \omega_e \pm \omega_H = \omega_e \pm 60$ MHz, indicating that the major portion of the electrons behave as fixed paramagnetic centers with dominating static dipolar interactions with the protons. This enhancement, referred to as the solid-state effect, is caused by simultaneous electron−proton flip-flip and flip-flop transitions, induced by the microwave irradiation. These transitions are normally forbidden but become nonzero as a result of the proton−electron dipolar interactions. The small nonzero enhancement observed at the electron Larmor frequency is due to a small Overhauser effect, and indicates that a portion of the protons experience time-dependent electron−proton interactions as well. It is possible that electron−electron spin-exchange interactions are responsible for this effect. A third maximum (e.g., approximately the same magnitude as the Overhauser effect) is present in each curve at a frequency offset intermediate between that of the solid state and the Overhauser contributions. This component is due to the thermal mixing effect and results from the EPR line being partially homogeneously broadened so that polarization transfer can arise from a combination of saturating the EPR line with the microwave irradiation, electron−electron flip-flop interactions, and electron−proton dipolar interactions.

To simulate the ^{1}H DNP enhancement curves the combined functional forms[31] of all enhancement mechanisms should be used. As a first approximation a set of Gaussian functions were used to simulate the contributions of the visible and dominant enhancement mechanisms. The origin of the fits were pairwise locked to $\omega_e \pm \omega_s$, $\omega_e \pm \omega_o$, and ω_e during the fitting process to take account of the solid state ($\omega_e \pm \omega_s$), direct thermal mixing ($\omega_e \pm \omega_o$), and Overhauser effect (ω_e), respectively. ω_o is the frequency where the direct thermal mixing effect becomes maximal. It is acknowledged that this simulation is an approximation since the direct and indirect thermal mixing mechanisms were not both individually included in the analysis. The approximations employ only a semiquantitative analysis of the mechanisms and relative contributions to the composite shape of the enhancement curve to illustrate the complexities of the several enhancement mechanisms. The enhancement factors measured at $\omega = \omega_e \pm 60$ MHz (the frequency of the solid-state effect) of the four doped samples are given in Table 3.

Several interesting observations are apparent from the data in Table 3. First, the largest contribution is that of the solid-state effect which varies with the doping level, e.g., the maximum value of 35 is observed at the 1.1% doping level and decreases to 15 at the 5% level. Second, the frequency ω_s at

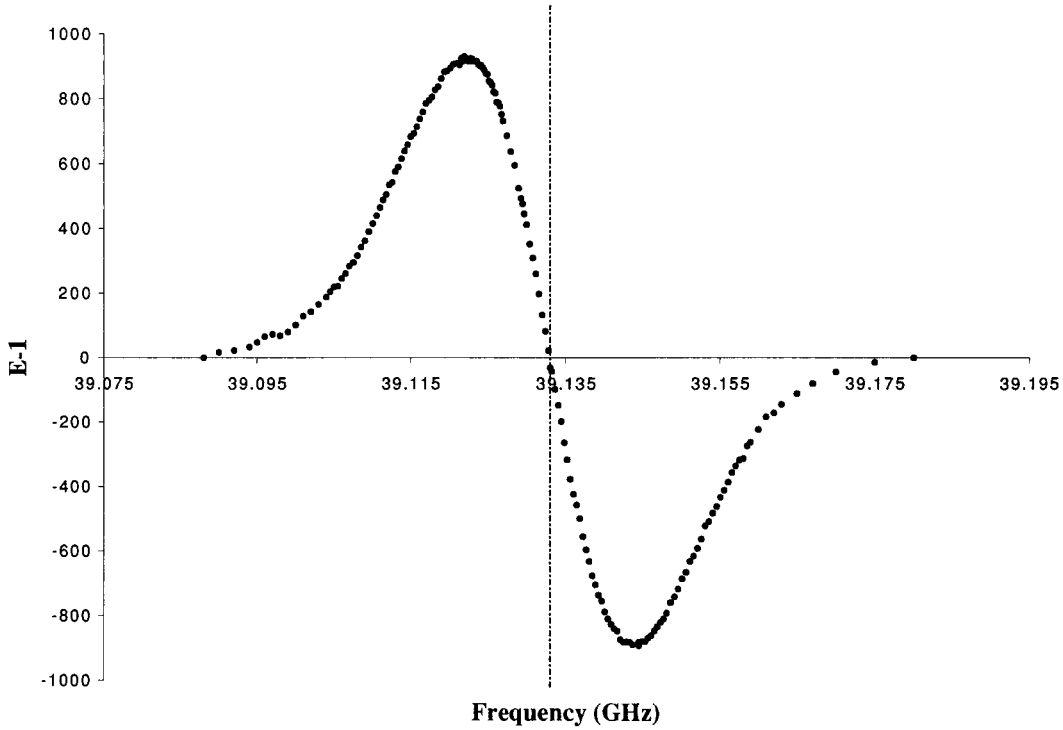

Figure 4. The ^{15}N DNP enhancement curve of 98% ^{15}N labeled carbazole doped with 1.1 wt % BDPA as a function of microwave irradiation frequency.

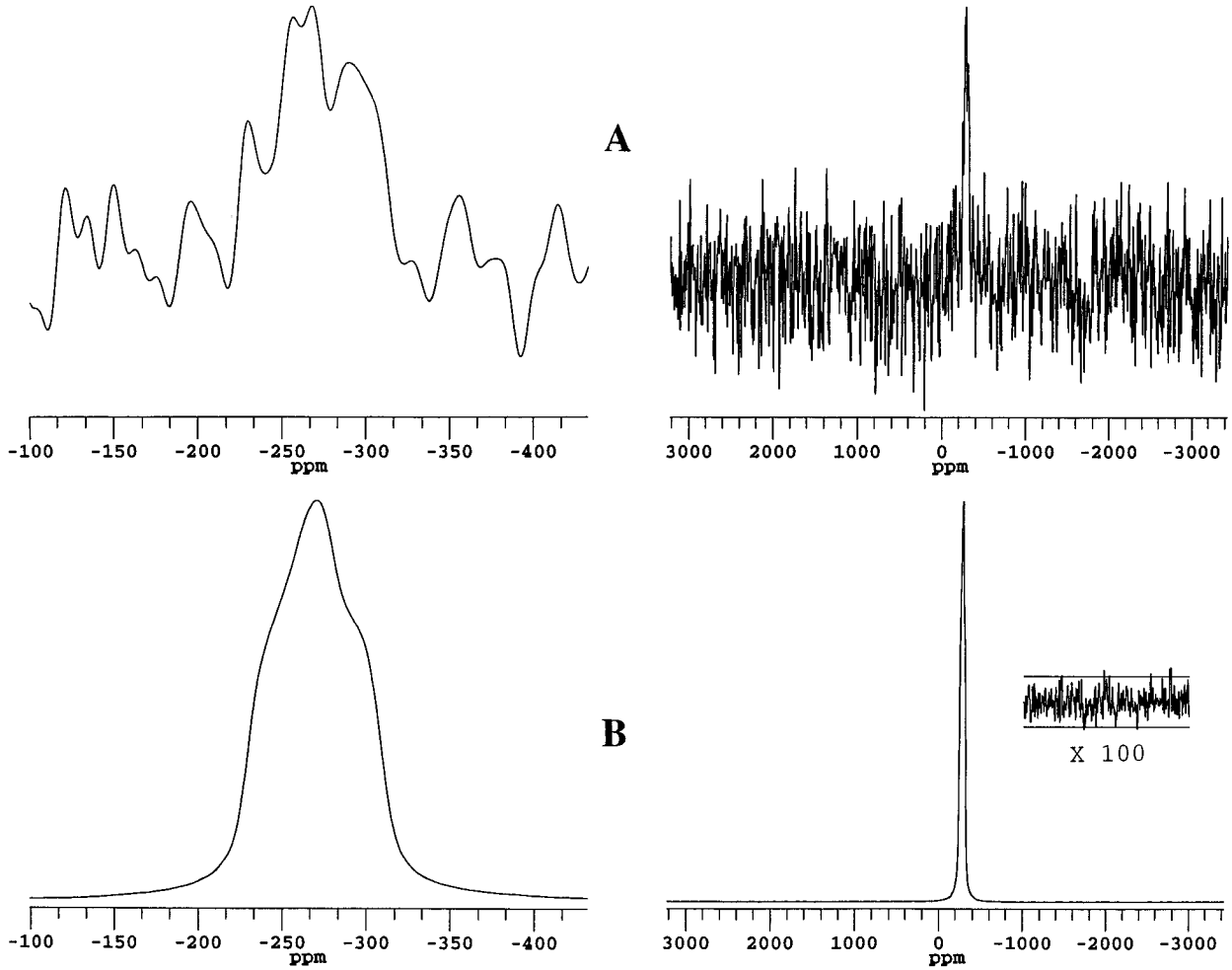

Figure 5. The room temperature ^{15}N spectrum of 98% labeled carbazole, doped with 1.1 wt % BDPA, obtained with a single pulse experiment. Top: normal single pulse experiment. The recycle delay time is 3000 sec and the number of scans is 48. The signal-to-noise ratio is 3.7. Bottom: Single pulse DNP experiment. The microwave frequency was 11 MHz lower than the electron Larmor frequency. The recycle delay time is 3000 sec and the number of scans is 16. The signal to-noise ratio is 1980. In both spectra a Lorentzian line broadening of 25 Hz was applied.

which the curve has maximum intensity changes from 59.3 to 57.9 MHz as the doping level increases. This apparent frequency shift is thought to be a manifestation of the change in relative contributions of the solid-state mechanism (which decreases) and that of the indirect thermal mixing mechanism which lies upfield from the maximal point in the solid-state enhancement curve and which (curve) overlaps with that of the solid-state effect (see Figure 3).

As the doping level increases it is also noted that the half-width of the solid state contribution increases while the enhancement decreases. The thermal mixing enhancement was simulated only in terms of the direct thermal mixing effect. The enhancement factor increases from a value of 3 at the 0.65% doping level and then is essentially constant at a value of approximately 6. The Overhauser enhancement is estimated at a value of 4 and appears to be independent of the doping level. Hence, the estimated enhancement factors due to the Overhauser and thermal mixing mechanisms appear to be largely independent of the doping level. However, the contribution from the solid-state effect is clearly related to the level of free radical doping.

2. ^{15}N NMR and DNP NMR. In principle DNP techniques can be used in two ways to enhance the ^{15}N NMR signal: (1) indirectly, by first enhancing the ^{1}H signal, and then transferring this enhanced polarization to the ^{15}N nuclei by cross polarization. This process is called DNP-CP;[10] (2) directly, by enhancing the ^{15}N polarization with the microwave irradiation without CP. In the second instance the ^{15}N signal is observed with a standard 90° pulse. This process is called single pulse DNP, or DNP-SP. Both methods have advantages and disadvantages. For instance, in DNP-CP the relatively short ^{1}H T_1 dictates the pulse repetition rate, which shortens the measuring time of an experiment. However, the interplay between the finite ^{1}H-^{15}N contact time and ^{1}H $T_{1\rho}$ can result in spectral distortions. This condition is avoided in a DNP-SP experiment. Moreover, in materials that do not contain abundant spins, the DNP-SP experiment is the only possible technique. For rare spins the DNP enhancement factors are usually considerably larger than those of protons[10] and, as discussed below, this is also the case for the ^{15}N DNP enhancement factors in carbazole. The ultimate consequence is a significant reduction in the number of spectral scans needed to perform a successful DNP-SP experiment.

The ^{15}N DNP enhancement curve, obtained via DNP-SP, for the 98% ^{15}N-labeled carbazole doped with 1.1 wt % BDPA is presented in Figure 4. The curve is completely anti-symmetrical, and the maximum enhancements occur at 39.133 ± 0.011 GHz. It has been shown[10] for rare spins that these maxima are mainly due to the direct thermal mixing effect. To determine the maximum ^{15}N DNP enhancement factor, single pulse experiments were performed on the same sample with and without DNP. The results are presented in Figure 5.

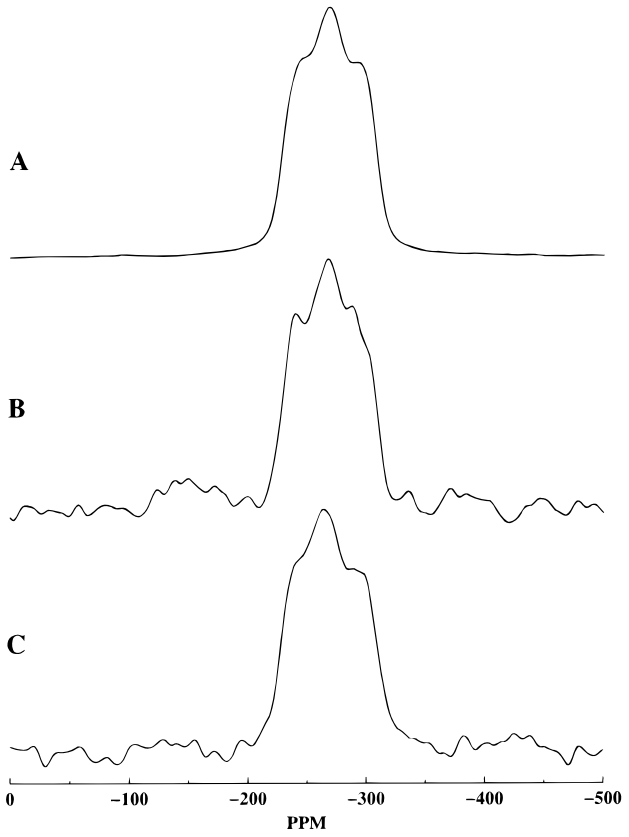

Figure 6. The ^{15}N spectrum of carbazole, doped with 1.1 wt % BDPA, obtained with CP and DNP-CP. (A) 98% ^{15}N labeled carbazole, DNP-CP. The microwave frequency was 60 MHz lower than the electron Larmor frequency. The proton DNP enhancement is 35; recycle delay time is 4 s; contact time is 0.5 ms; number of scans is 16. (B) 98% ^{15}N labeled carbazole, CP without proton DNP enhancement. The recycle delay time is 4 s; contact time is 0.5 ms; number of scans is 16. (C) Natural abundance ^{15}N spectrum, measured with DNP-CP at a temperature of 150 K. The proton DNP enhancement is 33; recycle delay time is 2 s; contact time is 0.5 ms; number of scans is 596. Different line shapes of the powder patterns still give equivalent chemical shift tensors.

The signal-to-noise ratio (S/N) of the spectrum without DNP is rather poor, resulting from a long ^{15}N spin−lattice relaxation time despite the doped sample. Therefore, only a few scans could be taken in an acceptable measuring time. Actually, the relaxation could be described rather accurately by $\exp[-(t/T_{1N})^{1/2}]$, which is typical for nuclei relaxed by paramagnetic centers in instances where the spin diffusion among the nuclei can be neglected.[10] The nitrogen T_{1N} was 340 s, and the recycle delay had to be taken very long (3000 s) in order to reach thermal equilibrium for the magnetization. It follows from the observed S/N ratio that the maximum ^{15}N DNP enhancement factor is at least 930, about 25 times larger than the ^{1}H DNP enhancement. With this large enhancement it is possible to obtain a ^{15}N spectrum with excellent S/N with only one scan. Similar DNP-SP experimental data were acquired from the ^{13}C spectra of carbazole and a ^{13}C-enhancement factor of approximately 800 was obtained.

Figure 6 shows ^{15}N spectra of carbazole obtained via the DNP-CP technique. Figure 6a and b displays the spectra of the ^{15}N labeled sample, doped with 1.1 wt % BDPA, obtained with and without proton DNP. These spectra illustrate the ^{15}N signal enhancement by the indirect ^{1}H DNP enhancement factor. Even though the ^{15}N enhancement is considerably reduced in the DNP-CP experiment (as compared to the DNP-SP experiment), a spectrum with a high S/N ratio can be obtained in a short time (about one minute in the DNP-CP case) since the recycle delay time can be made relatively short. The DNP-CP enhancement is sufficient that ^{15}N spectra can be obtained in a relatively short time (20 min) in unlabeled carbazole, as illustrated in Figure 6c. This experiment was performed at 150 K. At this temperature both the proton T_1 and DNP enhancement factor were the same as those observed at room temperature, but a factor of 2 increase in sensitivity is obtained as a result of the increased Boltzmann distribution.

TABLE 4: Carbazole ^{15}N Shift Tensor Principal Values[a]

sample and experiment	δ_{11}	δ_{22}	δ_{33}	δ_{avg}
DNP-CP natural abundance (1.4 T)	−223	−263	−314	−266.7
DNP-SP, ^{15}N labeled (1.4 T)	−227	−268	−309	−268.0
CP ^{15}N labeled (4.7 T)	−233	−266	−306	−268.3

[a] Values are in ppm with respect to nitromethane.

Finally, the chemical shift tensor principal values of samples doped at the 1.1% level are given in Table 4. The DNP-SP and DNP-CP data (on a ^{15}N labeled sample and natural abundance sample, respectively) give a sense of the errors that might be encountered in these two types of experiments. The maximum difference in the principal values of these two experiments is 5 ppm while the isotropic shift differs by only 1.3 ppm. These results are consistent within the experimental error for the analysis of static powder pattern data. The standard CP experiment was also performed on the ^{15}N labeled sample at 4.7 T in order to acquire a sufficient S/N ratio to obtain principal shift values of the nitrogen atom. These data are also given in Table 4 and are within experimental error of that obtained by DNP indicating that free radical doping does not significantly distort the tensor shift values.

Conclusions

It has been shown that doping polycrystalline carbazole with BDPA via the solvent evaporation technique has several advantages. First, doping reduces the nuclear relaxation time and second, it presents the possibility of enhancing the nuclear signals of both abundant and rare spins by means of DNP. Proton DNP enhancements of about 35 have been obtained, a SP ^{15}N DNP enhancement of at least 930 has been measured, and a comparable enhancement magnitude was found for the ^{13}C nuclei in the doped carbazole samples. These data demonstrate the feasibility of obtaining natural abundance ^{15}N NMR spectra in a reasonable time. For instance, with DNP-CP a natural abundance ^{15}N NMR spectrum with an adequate S/N ratio could be obtained in only 20 min. Though the ^{15}N relaxation time in the doped carbazole sample is still long, such a large ^{15}N SP DNP enhancement factor (e.g., several hundred) would be promising to allow the observation of nonprotonated nitrogens at the natural abundance level in a MAS experiment. Such ^{15}N MAS experiments in coals, for instance, have been very difficult[40] since the proton $T_{1\rho}$ may be very short while the cross polarization time for the nonprotonated nitrogens can be much longer.[1]

For carbazole the optimum doping level is about 1 wt % BDPA. At this level the proton T_1 is reduced from about 800 s to a very acceptable value of 2.2 s, whereas the proton $T_{1\rho}$ becomes 3.4 ms, which is sufficiently large to allow cross polarization experiments. At this doping level the proton DNP signal enhancement becomes maximal and line broadening in the rare spin spectra due to the presence of the radicals is not observed. The absence of line broadening was confirmed by comparing ^{13}C and ^{15}N CP and CPMAS data on doped (at the 1.1 wt % BDPA level) and undoped 98% ^{15}N labeled carbazole

on experiments carried out at 4.7 T. Within experimental error, the chemical shift anisotropy and the isotropic chemical shifts, as well as the line intensities and line widths, were the same in the doped and undoped samples.

In conclusion, doping crystalline solids such as carbazole with BDPA allows one to acquire rare spin NMR data on samples that would otherwise be very difficult or impossible at a magnetic field as low as 1.4 T without the enhancements provided by DNP techniques.

Acknowledgment. Support for this work was provided by NEDO (New Energy Development Organization), Pacific Northwest National Laboratory through contract 353465-A-5E, and the University of Utah. Additional support was provided by the Department of Energy under contract number DE-FG02-94ER14452 from the Division of Chemical Sciences of the Office of Basic Energy Sciences. RW was supported by an internal grant from the Pacific Northwest National Laboratory, a multi-program laboratory operated by Battelle Memorial Institute for the U.S. Department of Energy under contract DE-AC06-76RLO 1830.

References and Notes

(1) Solum, M. S.; Altmann, K. L.; Strohmeier, M.; Berges, D. A.; Zhang, Y.; Facelli, J. C.; Pugmire, R. J.; Grant, D. M. *J. Am. Chem. Soc.* **1997**, *119*, 9804.

(2) Duncan, T. M. A Compilation of Chemical Shift Anisotropies; The Farragut Press: Chicago, 1990.

(3) Mason, J. Nitrogen NMR, In *Encyclopedia of Nuclear Magnetic Resonance*; Grant, D. M., Harris, R. K., Eds.; John Wiley: London, 1996; p 3222.

(4) Anderson-Altmann, K. L.; Phung, C. G.; Mavromoustakos, S.; Zheng, Z.; Facelli, J C.; Poulter, C. D.; Grant, D. M. *J. Phys. Chem.* **1995**, *99*, 10 454.

(5) Strohmeier, M.; Orendt, A. M.; Facelli, J. C.; Solum, M. S.; Pugmire, R. J.; Parry, R. W.; Grant, D. M. *J. Am. Chem. Soc.* **1997**, *119*, 7114.

(6) Hu, J. Z.; Facelli, J. C.; Alderman, D. W.; Pugmire, R. J.; Grant, D. M. *J. Am. Chem. Soc.* **1998**, *120*, 9863.

(7) Abragam, A. *The Principles of Nuclear Magnetism*; Oxford University Press: London, 1961.

(8) Goldman, M. *Spin Temperature and NMR in Solids*; Oxford University Press: London, 1970.

(9) Abragam A.; Goldman, M. *Nuclear Magnetism: Order and Disorder*; Oxford University Press (Clarendon), London/New York, 1982.

(10) Wind, R. A.; Duijvestijn, M. J.; van der Lugt, C.; Manenschijn, A.; Vriend, *J. Prog. NMR Spectrosc.* **1985**, *17*, 33.

(11) Wind, R. A. DNP and High-Resolution NMR in Solids. In *Encyclopedia of Magnetic Resonance*; Grant, D. M., Harris, R. K., Eds. John Wiley & Sons: London; 1996, p 1798.

(12) Duijvestijn, M. J.; Van der Lugt, C.; Smidt, J.; Wind, R. A.; Zilm, K. W.; Staplin, D. C. *Chem. Phys. Lett.* **1983**, *11*, 25.

(13) Lock, H.; Wind, R. A.; Maciel, G. E.; Zumbulyadis, N. *Solid State Comm.* **1987**, *64*, 41.

(14) Maresch, G. G.; Kendrick, R. D.; Yannoni, C. S.; Calvin, M. E. *Macromolecules* **1988**, *21*, 3525.

(15) Singel, D. J.; Seidel, H.; Kendrick, R. D.; Yannoni, C. S. *J. Magn. Res.* **1989**, *81*, 145.

(16) Afeworki, M.; McKay, R. A.; Schaefer, J. *Macromolecules* **1992**, *25*, 4084.

(17) Afeworki, M.; Schaefer, J. *Macromolecules* **1992**, *25*, 4092.

(18) Afeworki, M.; Schaefer, J. *Macromolecules* **1992**, *25*, 4097.

(19) Afeworki, M.; Vega, S.; Schaefer, J. *Macromolecules* **1992**, *25*, 4100.

(20) Lock, H.; Maciel, G. E. *J. Mater. Res.* **1992**, *7*, 1.

(21) Li, L.; Qiu, J.; Hu, X.; Liu, Y.; Ye, C. *Sci. China* **1992**, *A4*, 419.

(22) Zhou, J.; Li, L.; Hu, H.; Yang, B.; Dan, Z.; Qiu, J.; Guo, J.; Chen, F.; Ye, C. *Solid State NMR* **1994**, *3*, 339.

(23) Hall, D. A.; Maus, D. C.; Gerfen, G. J.; Inati, S. J.; Becerra, L. R.; Dahlquist, F. W.; Griffin, R. G. *Science* **1997**, *276*, 930.

(24) Gerfen, G. J.; Becerra, L. R.; Hall, D. A.; Griffin, R. G.; Temkin, R. J.; Singel, D. J. *J. Chem. Phys.* **1995**, *102*, 9494.

(25) Becerra, L. R.; Gerfen, G. J.; Bellew, B. F.; Bryant, J. A.; Hall, D. A.; Inati, S. J.; Weber, R. T.; Un, S.; Prisner, T. F.; McDermott, A. E.; Fishbein, K. W.; Kreischer, K. E.; Temkin, R. J.; Singel, D. J.; Griffin, R. G. *J. Magn. Reson.* **1995**, *A117*, 28.

(26) Hu, J. Z.; Zhou, J.; Yang, B.; Li, L.; Qiu, J.; Ye, C.; Solum, M. S.; Wind, R. A.; Pugmire, R. J.; Grant, D. M. *Solid State NMR* **1997**, *8*, 129.

(27) (a) Ganapathy, S.; Naito, A.; McDowell, C. A. *J. Am. Chem. Soc.* **1981**, 103, 6011; (b) Bao-Lian, Y.; Ji-Wen, F.; Li, L.; Ye, C.; Hu, J. Z.; Pugmire, R. J.; Grant, D. M. *Acta Physica Sinica* **1998**, *7*, 106.

(28) Details of the DNP setup and the DNP probe will be submitted separately for publication.

(29) Wind, R. A.; Anthonio, F. E.; Duijvestijn, M. J.; Smidt, J.; Trommel, J.; De Vette, G. M. C. *J. Magn. Reson.* **1983**, *52*, 424.

(30) Wind, R. A.; Hall, R. A.; Jurkiewicz, A.; Lock, H.; Maciel, G. E. *J. Magn. Reson.* **1994**, *A110*, 33.

(31) Duijvestijn, M. J.; Wind, R. A.; Smidt, J. *Physica* **1986**, *138B*, 147.

(32) Peterson M. A.; Nilsson, B. L. *Synth. Commun.* **1999**, *29*, 3821.

(33) Manuscript in preparation.

(34) Gerstein, B. C.; Hu, J. Z.; Zhou, J.; Ye, C.; Solum, M. S.; Pugmire, R. J.; Grant, D. M. *Solid State NMR* **1996**, *6*, 63.

(35) Blumberg, W. E. *Phys. Rev.* **1960**, *119*, 79.

(36) Lowe, I. J.; Tse, D. *Phys. Rev.* **1968**, *166*, 279.

(37) Tse, D.; Lowe, I. J. *Phys. Rev.* **1968**, *166*, 292.

(38) Wind, R. A.; Jurkiewicz, A.; Maciel, G. E. *Fuel* **1989**, *68*, 1189.

(39) Clarke, P. T.; Spink, J. M. *Acta Crystallogr.* **1969**, *B25*, 162.

(40) Solum, M. S.; Pugmire, R. J.; Grant, D. M.; Kelemen, S. R.; Gorbaty, M. L.; Wind, R. A. *Energy Fuel* **1997**, *11*, 491−494.